J Therm Anal Calorim (2012) 109:933–938
DOI 10.1007/s10973-011-1809-x

Effect of ball-milling conditions on microstructure during production of Fe–20Mn–6Si–9Cr shape memory alloy powders by mechanical alloying

A. Dogan · H. Arslan

Received: 6 June 2011 / Accepted: 18 July 2011 / Published online: 3 August 2011

Abstract Phase transitions associated with Fe–20 wt% Mn–6 wt% Si–9 wt% Cr alloy during mechanical alloying and after subsequent annealing of that are studied experimentally. The conventional powder metallurgy route was used in preparing the sample. The milling time ranged from 5 to 20 h. Changes in microstructure as a function of milling time were investigated by using X-ray diffraction analysis, differential scanning calorimeter, and scanning electron microscopy. The grain sizes of powder milled are determined. The critical temperatures associated with the transformations are found to change with increasing ball-milling time.

Keywords Mechanical alloying · Martensitic phase transformation · Alloys · Annealing

Introduction

Fe–Mn–Si-based alloys have drawn much attention due to shape memory effect (SME) [1, 2, 3]. Fe–Mn–Si-based alloys have long been extensively studied since pronounced SME was discovered in a Fe–30Mn–1Si single crystal in early 1980s [2].

These alloys exhibit many advantages such as high strength, good plasticity, and low price. The shape memory effect in these alloys is derived from the transformation of stress-induced—martensite (hcp structure) being reversed into—parent austenite (fcc structure) upon heating.

A. Dogan · H. Arslan (✉)
Faculty of Arts and Sciences, Physics Department, Sutcuimam University, Kahramanmaras, Turkey
e-mail: hseyin_arslan@yahoo.com

In the past decades, extensive studies of the Fe–Mn–Si-based alloys (SMAs) focused on the improvement of their shape memory performance by means of composition design [4, 5, 6, 7, 8], thermomechanical training [5–15], and precipitation strengthening [15], etc. The thermomechanical training has proven to be the most effective way to improve the shape memory performance, but it may lead to increase in the production cost and difficulties involved in the fabrication of complex shapes. In recent years, Fe–Mn–Si-based SMAs have been widely developed because of their relatively low cost and simpler manufacturing process, compared to Cu-based and Ni–Ti SMA.

Fe–Mn–Si-based shape memory alloys (SMAs), which possess a low stacking fault energy (SFE), show γ to α', γ to ε, and ε to α' martensite transformations.

As early as 1984, Sato et al. [16] studied the SME in single crystal Fe–(20–32)Mn–(1–6.5)Si SMAs. Otsuka et al. [17] added Cr and Ni to Fe–Mn–Si SMAs to improve their corrosion resistance and thermoplasticity. They also studied systematically more than ten alloys with 13–31.5% Mn, 4.7–6.1% Si, 0–13.9% Cr, and 0–6.8%Ni. The composition of the shape memory alloy powder fabricated in this article is mainly determined from the literature just mentioned above with additional data from references [18, 19].

The purpose of this study is to evaluate mechanical alloying (MA) as a process to obtain Fe–20 wt% Mn–6 wt% Si–9 wt% Cr powder. It is well known that the main characteristic of these materials with shape memory effects is diffusionless phase transformation i.e., martensitic transformations. In this study, therefore, various ball-milling conditions were examined to find optimum conditions for fabricating the alloy powders just mentioned above with a large transformation temperature range by investigating the microstructure and transformation

behaviors of the powders. In addition, as a function of milling time, the morphological changes, transformation behavior, and crystal structures of the powders were investigated by means of SEM, DSC, and XRD, respectively.

Experimental

Fe (99.99% pure, −100 +325 mesh in size), Mn (99.99% pure, −100 +325 mesh in size), Si (99.999% pure, −100 +325 mesh in size), and Cr (99.99% pure, −100 +325 mesh in size) powders were used as the raw materials. Nominal composition was set to an weight percent of Fe–20 wt% Mn–6 wt% Si–9 wt% Cr. The experiments are carried out in KSU, Art and Science Faculty, Research Laboratory. The milling medium and devices used were made from hardened steel. A planetary ball mill Fritsh Pulverisette with four stainless steel vials was used in the MA process. The vial contained hardened steel balls with weight of 4 g. The ball to powder weight ratio (BRP) was 20:1 (200 and 10 g, respectively). The rotational velocity is 300 rev/min. To prevent overheating, the device was turned on for 15 min and then it was turned off for 30 min for cooling off. A protective argon atmosphere was maintained during the milling process in mills. Milling time intervals were set to 0, 5, 10, 15, and 20 h. The milled products were characterized using a diffractometer model Philips X-Pert PRO and operated with a filtered Cu-Kα radiation of 0.1542 nm. In order to investigate the transformation behaviors and temperatures, the differential scanning calorimetry (Perkin-Elmer, DSC-4000) is carried out at the heating and cooling rate 20 K/min. The milled products were also characterized by scanning electron microscope (SEM model JEOL JSM-5500LV).

Results and discussion

The diffractograms of the Fe–20Mn–6Si–9Cr alloy powder milled for 0, 5, 10, 15, and 20 h are shown in Fig. 1. The shape and diffraction angle of the diffraction peaks were observed to change with increasing milling time. After 5 h of milling, Fe, Mn, Si, and Cr peak heights decreased indicating that an iron solid solution had started forming. The Fe and Cr peaks displaced slightly to the low angles, indicating an increase in the lattice parameter of Fe, due to dissolution of Mn, Si, and Cr atoms into Fe matrix and the Mn, Si, and Cr peaks decrease on increasing the milling time.

As for shape of the diffraction peaks, in the case of the XRD pattern obtained from the powders milled for more than 5 h, the diffraction peaks broadened, and the width of the diffraction peaks increased with increasing milling

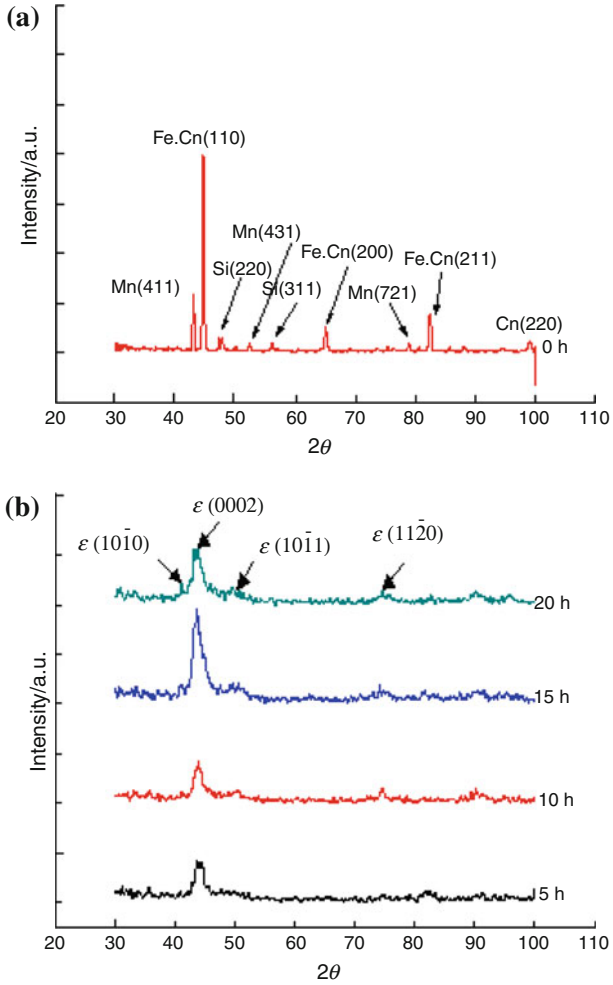

Fig. 1 Set of XRD pattern of Fe–20Mn–6Si–9Cr powder mixture as a function of milling time for **a** 0, **b** 5, 10, 15, and 20 h

time. From Fig. 1, it is thought that the broadening in the diffraction peaks is ascribed to deformations and refinements in microstructures by ball milling.

It can be seen from the experimental results mentioned above that the Mn, Si, and Cr contents play an important role in the phase transformation tendency during mechanical alloying of Fe–20Mn–6Si–9Cr powders. During mechanical alloying of Fe–20Mn–6Si–9Cr, with the increase of milling time, more and more solute atoms dissolve in the iron, accompanied by the reduction in grain size and the increase of internal strain, Therefore, the transformation takes place. In order to accommodate the presence of extra Mn, Si, and Cr in the iron lattice and the increase of strain induced by mechanical alloying, a part of energy can be provided by mechanical alloying to transform the lattice from a highly strained fcc-phase (γ) into hcp-phase (ε) with greatly reduced strain. The average grain size of powders can be determined by using the Scherrer formula: $t = \frac{0.9\lambda}{B\cos\theta}$, where λ is the wavelength of

X-rays, θ is the Bragg angle, and B is the peak width at half-maximum (FWHM). The peak broadening (B) is caused by three factors: (a) instrumental broadening, (b) broadening due to strain, and (c) broadening due to fine grain size (gs), and can be written as: $B_{\text{total}} = B_{\text{I}} + B_{\text{S}} + B_{\text{gs}}$. B_{I} is determined experimentally, and broadening due to strain can be written as $\varepsilon \tan \theta$, where ε is the lattice strain. If the instrumental broadening is neglected, we get $B_{\text{total}} = \frac{0.9\lambda}{t\cos\theta} + \varepsilon\tan\theta$. For different values of the angle θ, the magnitude of lattice strain ε can be determined from the slope of the plot of $B\cos\theta$ versus $\sin\theta$. Due to the extremely small size of the crystallites, which are formed by local relaxation of distorted lattice structure, the residual plastic strain is expected to be negligible. Therefore, the crystallite size can be calculated readily by the simplified Scherrer formula [20]. Grain size was evaluated from the breadth of the XRD martensite peaks. Results show that particle size in the new phase decreases to about 0.1 μm quickly after 20 h of high energy milling (Fig. 2).

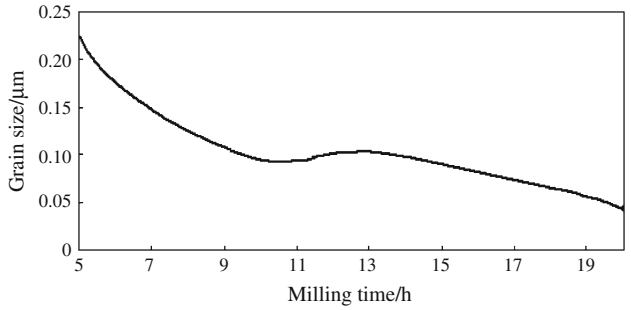

Fig. 2 Grain size versus milling time

The DSC curves registered during the heating of the powders mechanically alloyed for 0, 5, 10, 15, and 20 h are shown in Fig. 3. An endothermic peak effect is visible, which is a broad one in the temperature range 373–573 K. On the other hand, the DSC scan of the Fe–20Mn–6Si–9Cr alloy powder milled for 20 h after annealing at 1323 K for 30 min is shown in Fig. 4. The exothermic and endothermic event during cooling and heating were detected at ~348 and 598 K, respectively. It is found from the calculations performed by some researchers [21, 22] that M_{s} (martensite start temperature) and A_{s} (austenite start temperature) are 311 and 434 K, respectively. On the other hand, it is reported that A_{f} (austenite finish temperature) is 644 K, which is also an agreement with the prediction in the Ref. [23, 24]. For example, in order to explain the effects just mentioned above associated with the powder for milled 10 h, the samples annealed up to 373, 423, 473, 523, 573, 673, and 1323 K for 30 min subsequent quenched in ice-brine to retain hcp phase were subjected to XRD studies. Figure 5 shows the XRD patterns of the samples after 10 h of MA and after MA followed by heating up to range 373–1323 K. After heating the MA

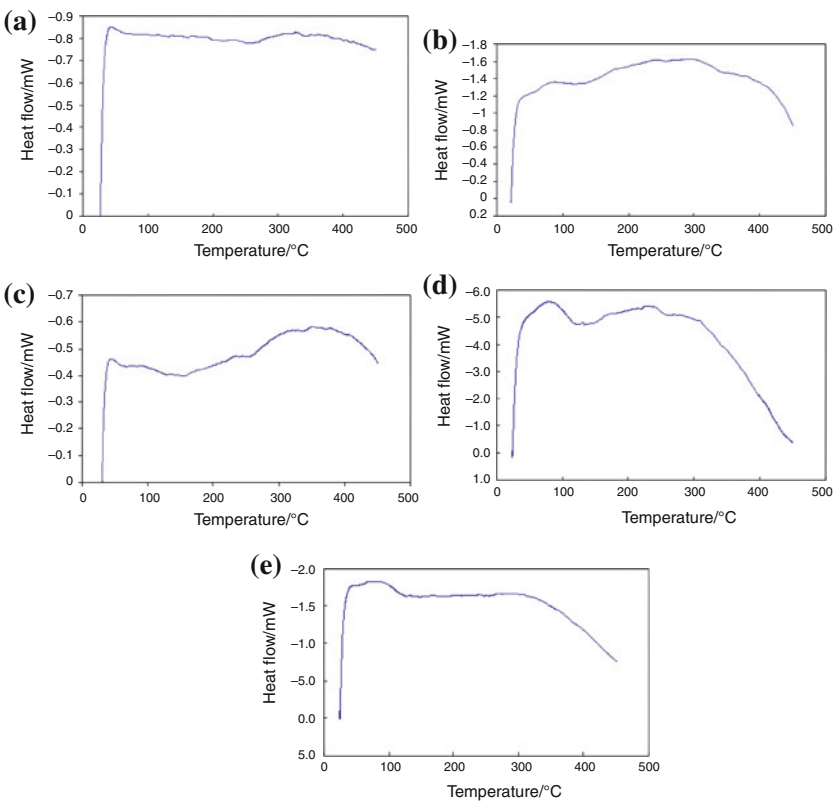

Fig. 3 The DSC curves registered during the heating of the powders mechanically alloyed for **a** 0, **b** 5, **c** 10, **d** 15, and **e** 20 h

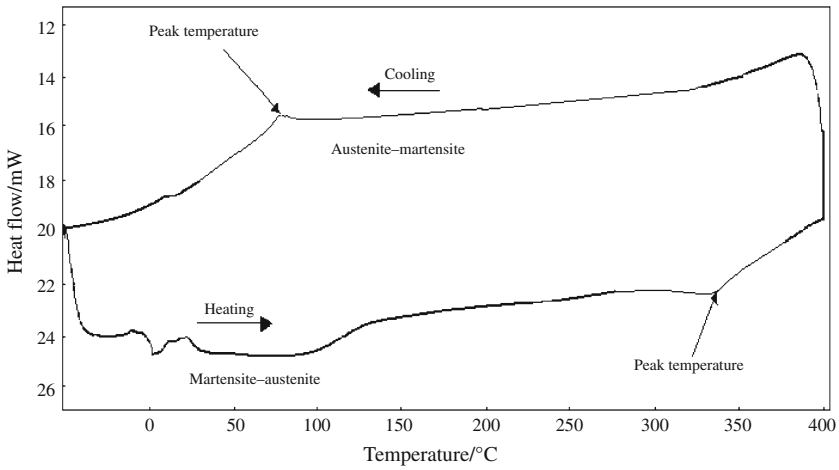

Fig. 4 DSC curves of Fe–20Mn–6Si–9Cr alloy powder (milled 20 h + annealed at 1323 K for 30 min)

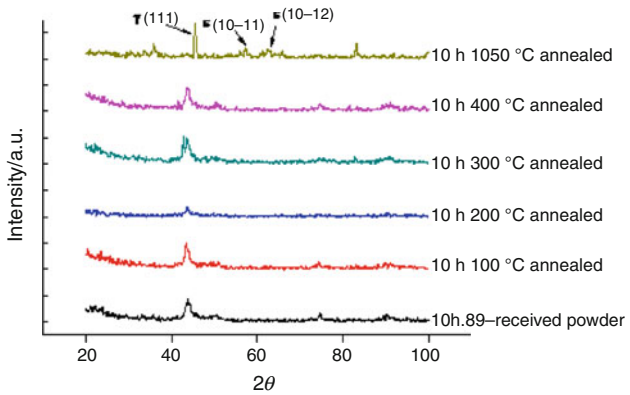

Fig. 5 The XRD peaks as seen that of 10 h milled powder alloy which were annealed different temperatures and subsequent quenched in ice-brine to retain hcp phase

powders up to 473 K, only crystallization peaks of the milled powder for 10 h are observed, however much narrow than after MA only. Heating the sample to the higher temperature leads to the appearance of a new phase peaks in the spectrum. The new peak observed at the milling time for 10 h suggests the formation of a solid solution. On the other hand, the high temperature XRD peaks can be attributed to the martensite formation. Thus, it is seen from the annealed sample at 1323 K for 30 min that the sharply peaks, $\varepsilon(10\bar{1}0)$, $\varepsilon(0002)$, $\varepsilon(10\bar{1}1)$, and $\varepsilon(11\bar{2}0)$ have structure of a new phase i.e., martensite phase. Using the standard peaks associated with austenite and martensite, the lattice parameters of these phase are calculated as $a_\gamma = 0.3468$ nm, $a_\varepsilon = 0.2947$ nm, and $c_\varepsilon = 0.4813$ nm.

SEM images allow studying the shape and the size of powder particles (Fig. 6). This figure shows the

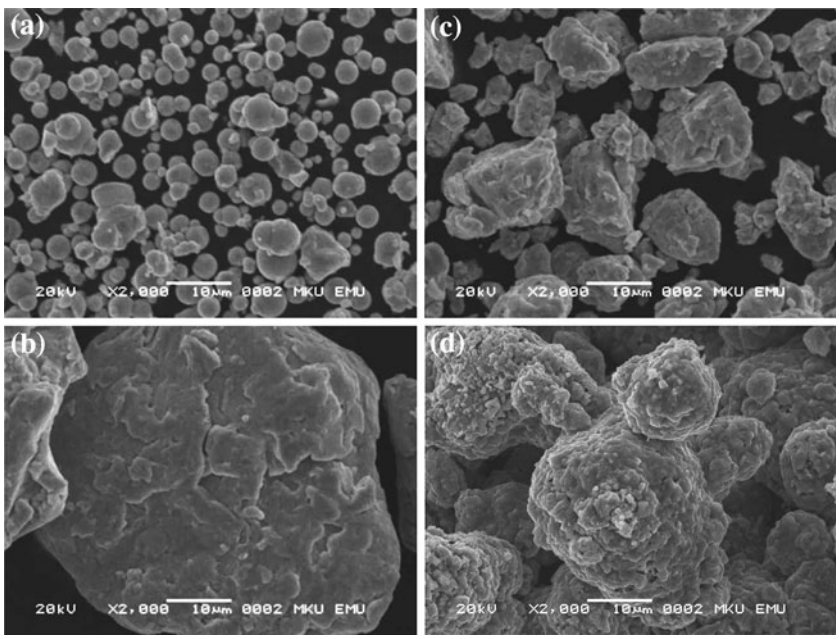

Fig. 6 Scanning electron micrograph of Fe–20Mn–6Si–9Cr powder mixture milled for **a** 0, **b** 10, **c** 20, and **d** 20 h, annealing 30 min at 1323 K subsequent quenched in ice-brine to retain hcp phase

micrographs of 0, 10, and 20 h milled powder as well as annealed (at 1323 K for 30 min) product of 20 h milled powder. The figure shows changes in the morphologies of powders which occurred during ball milling. After 0 h ball milling, however, elemental Fe, Mn, Si, and Cr powders were seen to be deformed and then to be agglomerated. By increasing the milling time further, the shape of the agglomerated powders becomes a globular shape, for example 10 h, as can be seen in Fig. 6b. At 20 h, by collision one another, it was seen that the particles of globular shape have broken and reduced. It can be seen from these figures that there are broad ranges of particle size nearly from 3 to 35 μm, induced by ball milling. Moreover, It can also be observed from these figures that the particle size, or may be clusters of several particles, has increased from 0 to 10 h then again decreased in 20 h.

Conclusions

In this study, Fe–20 wt% Mn–6 wt% Si–9 wt% Cr alloy is prepared by mechanical alloying. It is seen from the annealed sample at 1323 K for 30 min that the sharply peaks have structure a new phase which is called as martensite phase. The lattice parameters of the phases observed during the mechanical alloying are determined as $a_\gamma = 0.3468$ nm, $a_\varepsilon = 0.2947$ nm, and $c_\varepsilon = 0.4813$ nm ($c_\varepsilon/a_\varepsilon = 1.633$) by using the standard peaks associated with austenite and martensite phases. In addition, it is emphasis that the formation of martensite phase during the mechanical alloying depends on strictly the milling time. Results show that the particle size in the new phase, which is evaluated from the breadth of the XRD characteristic peaks, decreases to about 0.1 μm quickly after 20 h of high energy milling (Fig. 2). Powders fabricated with a milling time of more than 0 h were a mixture of Fe, Mn, Si, and Cr solid solution. It was found that the optimum ball-milling time at the linear velocity of 300 rev/min for fabricating Fe–20 wt% Mn–6 wt% Si–9 wt% Cr alloy powders was 20 h.

The basic analysis which determine the thermodynamic structure and phase transitions are done by DSC technique [25]. In recent years, it is focused on the mechanical alloying since the purpose of this method improves the thermomechanical properties of the alloys treated in a lot of studies [26, 27].

Acknowledgements The authors are pleased to acknowledge the financial support of this research by KSU under Grant No. 2008/3-30.

References

Murakami M, Otsuka H, Suzuki HG, Matsuda S. In: Proceedings of ICOMAT-86, The Japan Institute of Metals. pp 985–990; 1986.

Sato A, Chisima E, Soma K, Mori T. Shape memory effect in $\gamma \rightleftarrows \varepsilon$ transformation in Fe–30Mn–1Si alloy single crystals. Acta Metal. 1982;30:177–83.

Krindi T, Sari U, Dikici M. The effects of pre-strain, recovery temperature, and bending deformation on shape memory effect in an Fe–Mn–Si–Cr–Ni alloy. J Alloy Compd. 2008;475:145–50.

Wang XX, Zhao LC. The effect of thermal-mechanical training on the formation of stress-induced ε martensite in an Fe–Mn–Si–Ni–Co alloy. Scr Metall Mater. 1992;26:1451–6.

Soderberg O, Liu XW, Yakovenko PG, Ullakko K, Lindroos VK. Corrosion behaviour of Fe–Mn–Si based shape memory steels trained by cold rolling. Mater Sci Eng A. 1999;273–275:543–8.

Bliznuk VV, Gavriljuk VG, Shanina BD, Konchits AA, Kolesnik SP. Effect of nitrogen and carbon on electron exchange and shape memory in a Fe–Mn–Si base shape memory alloy. Acta Mater. 2003;51:6095–103.

Kubo H, Nakamura K, Farjami S, Maruyama T. Characterization of Fe–Mn–Si–Cr shape memory alloys containing VN precipitates. Mater Sci Eng A. 2004;378:343–8.

Lin HC, Lin KM, Lin CS, Ouyang TM. The corrosion behavior of Fe-based shape memory alloys. Corros Sci. 2002;44:2013–26.

Kajiwara S. Characteristic features of shape memory effect and related transformation behavior in Fe-based alloys. Mater Sci Eng A. 1999;273–275:67–88.

Li H, Dunne D, Kennon N. Factors influencing shape memory effect and phase transformation behaviour of Fe–Mn–Si based shape memory alloys. Mater Sci Eng A. 1999;273–275:517–23.

Jiang BH, Tadaki T, Mori H, Hsu TY. In situ TEM observation of gamma-ε martensitic transformation during tensile straining in an Fe–Mn–Si shape memory alloy. Mater Trans JIM. 1997;38:1072–7.

Jiang BH, Qi XA, Zhou WM, Xi ZL, Hsu TY. The effect of nitrogen on shape memory effect in Fe–Mn–Si alloys. Scr Metall Mater. 1996;34:1437–40.

Xia RD, Liu GW, Liu T. The effect of thermal training on prestrained Fe–30Mn–6Si–5Cr shape memory alloy. Mater Lett. 1997;32:131–6.

Lin HC, Lin KM, Wu SK, Wang TP, Hsia YC. Effects of thermo-mechanical training on a Fe59Mn30Si6Cr5 shape memory alloy. Mater Sci Eng A. 2006;438–440:791–5.

Stanford N, Dunne DP. Thermo-mechanical processing and the shape memory effect in an Fe–Mn–Si-based shape memory alloy. Mater Sci Eng A. 2006;422:352–9.

Sato A, Chisima E, Yamaji Y, Mori T. Orientation and composition dependencies of shape memory effect in Fe–Mn–Si alloys. Acta Metall. 1984;32:539–47.

Otsuka H, Yamada H, Tanahashi H, Maruyama T. Fe–Mn–Si based shape memory alloys. Mater Sci Forum. 1990;56–58:655–60.

Yang JH, Chen H, Wayman CM. Development of Fe-based shape memory alloys associated with face-centered cubic hexagonal close-packed martensitic transformations 1. Shape memory behavior. Metall Mater Trans. 1992;23A:1431–7.

Tomota Y, Nakagawara W, Tsuzaki K, Mori T. Reversion of stress-induced epsilon-martensite and 2-way shape memory in Fe–24Mn and Fe-24Mn–6Si alloys. Scr Metall Mater. 1992;26:1571–4.

Chittineni K, Bhat DG. X-ray diffraction investigation of the formation of nanostructured metastable phases during short-duration mechanical alloying of Cu–Al powder mixtures. Mater Manuf Process. 2006;21(5):527–33.

Zhao C. Relationships between martensite transformation temperatures, compositions in Fe–Mn–Si-based shape memory alloys. Proc Inst Mech Eng. 2000;214(Part L3):173–6. doi:10.1177/146442070021400306.

Dogan A, Ozer T. Determination of martensite transformation temperatures associated with Fe–Mn–Si–Ni–Cr–Ce–Ti–N shape memory alloys. Can Metall Quart. 2005;44:555–62.

Gavriljuk VG, Bliznuk VV, Shanina BD, Kolesnik SP. Effect of silicon on atomic distribution and shape memory in Fe–Mn base alloys. Mater Sci Eng A. 2005;406:1–10.

Wang Z, Zhu J. Cavitation erosion of Fe–Mn–Si–Cr shape memory alloys. Wear. 2004;256:66–72.

Petrovic DS, Klancnik G, Pirnat M, Medved J. Differential scanning calorimetry study of the solidification sequence of austenitic stainless steel. J Therm Anal Calorim. 2011;105:251–7. doi: 10.1007/s10973-011-1375-2.

Bonastre J, Escoda L, Gonzales A, Sunol JJ. Influence of Ni content on Fe–Nb–B alloy formation. J Therm Anal Calorim. 2007;88: 83–6.

Sunol JJ, Gonzales A, Escoda L, Vilaro A. Curie temperature in Fe(Ni)Nb based mechanically alloyed materials. J Therm Anal Calorim. 2005;80:257–61.